ORIGINAL ARTICLE

lajss.org© Latin American Journal of Solids and Structures

www.lajss.org

Identification of cracks in low-speed rotating slender cracked beams using frequencies and artificial rabbit algorithm

Belén Muñoz-Abella[a]*, Lourdes Rubio[a], Patricia Rubio[a]

[a]University Carlos III of Madrid. Dept. Ingeniería Mecánica. Avda de la Universidad, 30, 28223 Madrid, Spain. E-mail: mmunoz@ing.uc3m.es, lrubio@ing.uc3m.es, prubio@ing.uc3m.es

*Corresponding author

https://doi.org/10.1590/1679-78257954

Abstract

This article aims to identify the presence of cracks in slender rotating beams (Euler Bernoulli) from the dynamic behaviour of cracked beams operating at low rotational speeds. For this purpose, the behavioural model of the cracked rotating beam developed by the authors in previous works is shown. The results of the mathematical model developed (natural frequencies) feed a novel meta-heuristic optimisation algorithm based on the survival tactics of rabbits against their predators: Artificial Rabbit Optimization (ARO). The application of this algorithm to the first two natural frequencies of vibration obtained with the analytical model and contrasted in previous works gives rise to the identification of the characteristic parameters of the crack contained in the beams. The estimation of the parameters: position along the beam and crack depth, show a high similarity with the initial data, which allows validating the application of the optimisation algorithm to the identification of cracks in this type of component as a first approach to a health monitoring method for more complex rotating cantilever beam structures.

Keywords

Rotating beams, crack identification, artificial rabbit optimization, health monitoring

Graphical Abstract

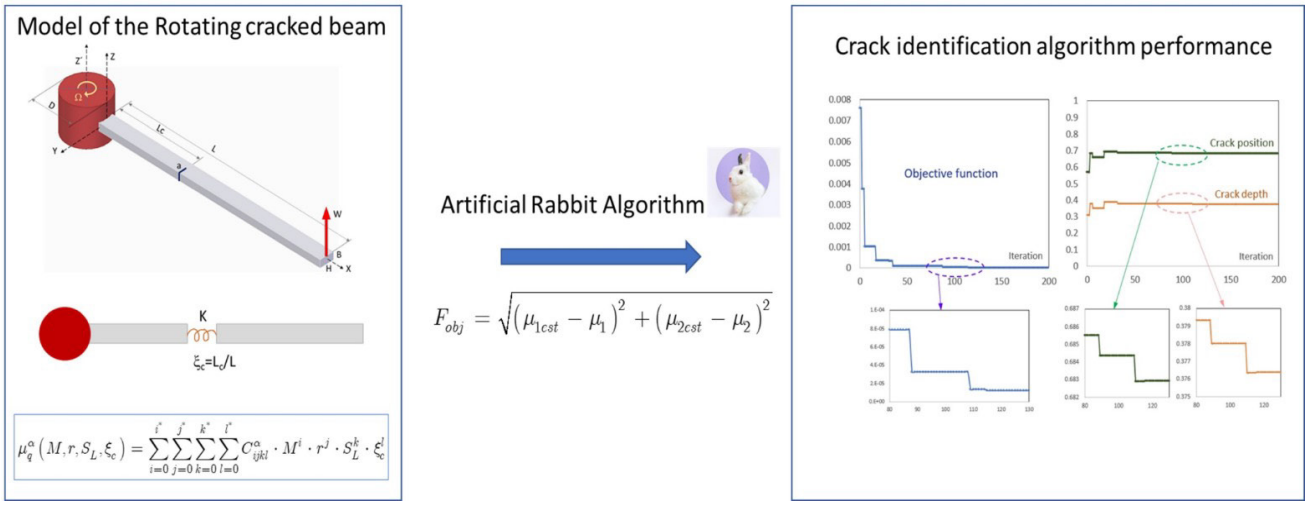

Received: November 30, 2023. In revised form: January 10, 2024. Accepted: January 16, 2024. Available online: January 24, 2024.
https://doi.org/10.1590/1679-78257954

1 INTRODUCTION

In most strategic sectors such as the transport and energy industries, there are mechanical components that can be represented and simplified as rotating beams. The most typical and significant cases are wind turbine blades, helicopter blades and open engines.

The working conditions of these components (extreme temperatures, aggressive media or cyclical wind loads) combined with possible manufacturing defects (sometimes invisible) can lead to the appearance and propagation of cracks and defects that seriously affect the operation of the device in which they are located, as well as causing risks to installations and machine operators. It is of great interest to detect defects when they are incipient as this can reduce the risks and costs associated with possible catastrophic failure of the component. However, the detection and identification of defects in their early stages is complex, so detection and identification techniques (position and severity) are highly recommended. Before having these procedures available, it is necessary to know the behaviour of rotating blades with defects to be able to compare this behaviour with that of intact blades and to determine the parameters that affect this behaviour. In this regard, it should be mentioned that the number of studies on the behaviour of cracked rotating blades is limited (Chen and Chen 1988; Wauer 1991; Banerjee and Pohit 2014; Lee and Lee 2017; Yashar et al. 2018; Valverde-Marcos et al. 2022).

The reason for knowing the dynamic behaviour of rotating beams lies in the fact that cracks (or defects in general) modify this behaviour and, in particular, modify the natural frequencies of the component. The variation of the natural frequencies of the damaged component compared to the intact one makes it possible to detect the presence of the defect. In general, the presence of a crack (or defect) in a beam produces an increase in its flexibility which results in a reduction of the natural frequency of vibration, see for example the works of Fernández-Sáez et al. (1999) or Loya et al. (2006).

In contrast to static beams, the dynamic behaviour of rotating beams depends not only on the geometrical and material characteristics of the beam but also on the centrifugal force that arises due to the rotation. Furthermore, this centrifugal force is not constant throughout the beam but depends on the distance to the centre of rotation. Another special feature of the dynamic behaviour of rotating beams is that there are directions for their study: “chordwise”, in the plane of rotation, and “flapwise”, outside the plane of rotation. In both intact and defective beams, the presence of this centrifugal force results in an increase of the natural frequency in both directions like in Lee and Lee (2017), Wauer (1991), Valverde-Marcos et al. (2022), Chen and Chen (1988), Yashar et al. (2018), Banerjee et al. (2014) and Bhat (1986).

In the case of cracked rotating beams, the two previously mentioned effects occur: on the one hand a decrease of the natural frequencies as a consequence of the presence of the cracks and on the other hand an increase of the frequency as a consequence of the centrifugal force. The fact that the effects compensate each other makes it difficult to detect the damage (see for instance Lee and Lee 2017; Valverde-Marcos et al. 2022; Muñoz-Abella et al. 2022a). It is of particular interest to analyse the behaviour at rotational speeds below 10 rad/s, those close to the behaviour of some real mechanical systems (wind engines), as it differs from that at higher rotational speeds (Muñoz-Abella et al. 2022a) so that specific studies should be done.

The estimation of crack characteristics from the knowledge of the dynamic behaviour of cracked elements is the inverse problem, as opposed to the direct problem explained above. Different methods and tools have been applied to address this problem. Of all of them, neural networks (Mohammed et al. 2014; Muñoz-Abella et al. 2020; Bilotta et al. 2023) currently occupy a prominent place in comparison with conventional optimisation techniques (Suh et al. 2000; Shekar 2004; Rubio 2009), or those based on constructive algorithms based on vibration problems (Fernández-Sáez et al. 2017; Rubio et al. 2018) or on genetic algorithms or other optimization methods (Maity and Tripathy 2005; Muñoz-Abella et al. 2018; Ramezani and Bahar 2021; Muñoz-Abella et al. 2022a, Gordan et al. 2017, Jahangiri et al. 2016, Marques et al. 2018). However, there are some methods whose use is currently gaining more strength with the development of AI.

This is the case of meta-heuristic algorithms that are increasingly used to solve optimisation problems in all fields of engineering. As indicated by Wang et al. (2022) in their extensive and comprehensive article, most of them are inspired by nature. These authors divide them into five types: evolutionary, swarm-based, based on physics and chemistry, and based on human behaviour.

In particular, swarm-based algorithms are inspired by the behaviour of swarms in nature (i.e. Ertenlice and Kalayci 2018). Since the mid-1990s, different algorithms of this type have been used to solve mathematical and engineering problems, including the well-known particle swarm optimisation (PSO), inspired by the behaviour of flocks of birds (Eberhart and Kennedy 1995) or others based on the behaviour of fireflies (Yang 2010), whales (Mirjalili and Lewis 2016), bees (Karaboga and Akay 2009), manta rays (Zhao et al. 2020), horses (Naruei and Keynia 2022) and rabbits (Wang et al. 2022; Alsaiari et al. 2023, Alamir et al. 2023, Nguyen et al. 2024), among others.

This paper presents a methodology for the identification of cracks in rotating, at low rotation velocities, Euler Bernoulli beams based on the novel optimisation algorithm called the Artificial Rabbit Algorithm. It is therefore the solution of an inverse problem in which the objective function is an expression that comes from the solution of the direct problem of integration of the equation of motion previously developed by the authors. To carry out the research, the commercial MATLAB code and a specific toolbox developed for the algorithm (Wang et al. 2022) have been used.

The input data comes from both the mathematical model of the behaviour of the cracked rotating beam, the same as in Muñoz-Abella et al. (2022a) and in Muñoz-Abella et al. (2023), for cases obtained with the model and for cases where a white error has been considered in the input data.

The proposed methodology would allow estimating the position and crack size of cracked Euler Bernoulli rotating beams at low rotating velocities simulating wind turbine or helicopter blades from the natural frequencies of the component, allowing estimation of the component's life.

2 STATEMENT OF THE DIRECT PROBLEM

2.1 Cracked Euler Bernoulli rotating beam model

A cracked Euler Bernoulli beam of uniform rectangular cross-section with double symmetry and with the following geometrical properties is considered: Length L, thickness B and depth H. The beam rotates with a constant speed Ω around an axis perpendicular to the longitudinal axis of the beam, as shown in Figure 1. The beam has a straight-fronted crack of depth a, located at a distance Lc from the point of contact with the hub. The cube has a diameter of D, at the centre of which the reference frame (X´, Y´, Z´) for the beam rotation is located, while the reference frame of the beam is located at the beam-hub contact point.

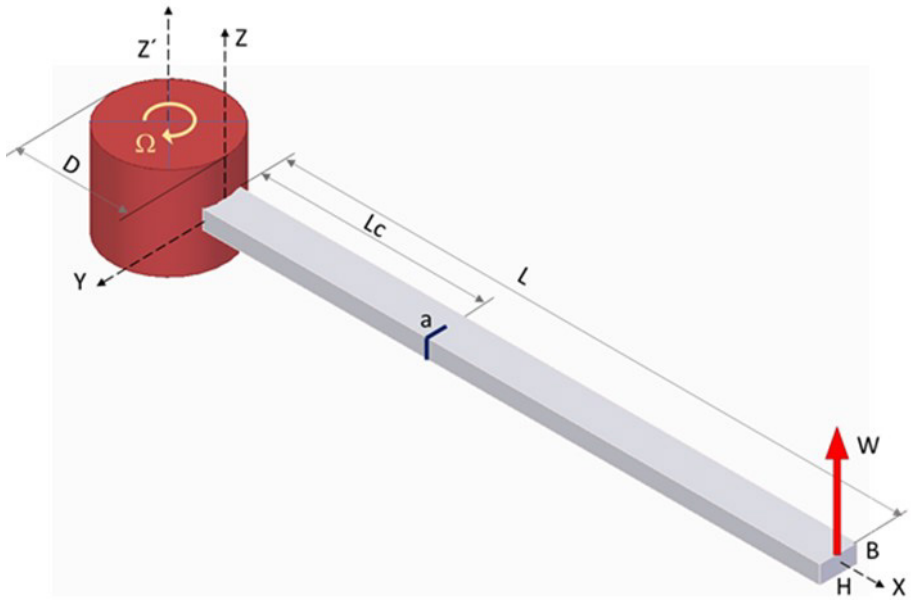

Figure 1 Schematic representation of the cracked rotating beam.

The differential equation governing the dynamic behaviour of the rotating beam, is valid only for slender beams because it ignores the effects of shear deformation and rotatory inertia (Banerjee et al., 2006 and Lee and Lee, 2017) can be expressed according to the expression eq. (1).

$$\rho A\frac{\partial^2 W(X,t)}{\partial t^2}+\frac{\partial^2}{\partial x^2}\left(EI\frac{\partial^2 W(X,t)}{\partial X^2}\right)-\frac{\partial}{\partial X}\left(P(X)\frac{\partial W(X,t)}{\partial X}\right)=0 \tag{1}$$

Where t is the time, ρ is the density, E is Young's modulus, I is the moment of inertia of the section and A is the cross-section area. On the other hand, P(X) is the centrifugal force which appears as a consequence of the rotational speed of the beam and has the form, Eq. (2):

$$P(X) = \int_X^L \rho A \Omega^2 (X + R) dX \tag{2}$$

The integration of the equation is verified by the method of separation of variables. Eq. (1) can then be expressed with dimensionless variables as follows:

$$\frac{d^4 w}{d\xi^4} - M^2 \frac{d}{d\xi}\left(\left(r(1-\xi) + \frac{1}{2}(1-\xi^2)\right)\frac{dw}{d\xi}\right) - \mu^2 w = 0 \tag{3}$$

Where the dimensionless variables are given by:

$$\xi = \frac{x}{L};\ r = \frac{R}{L};\ \alpha = \frac{a}{H};\ \mu = \sqrt{\frac{\rho A L^4}{EI}}\,\omega;\ M = \sqrt{\frac{\rho A L^4}{EI}}\Omega;\ S_L = \sqrt{\frac{AL^2}{I}} \tag{4}$$

In the case of a cracked beam, the equation of motion is divided into two equations, one for each span before and after the crack (equation 5). The connection between the two spans is verified by a massless rotational spring (see Figure 2) whose stiffness is related to the loss of stiffness of the beam at the cracked section, K according to Chondros et al., 1998, Eq. (6).

$$\begin{aligned} &\frac{d^4 w_1}{d\xi^4} - M^2 \frac{d}{d\xi}\left(\left(r(1-\xi) + \frac{1}{2}(1-\xi^2)\right)\frac{dw_1}{d\xi}\right) - \mu^2 w_1 = 0 \qquad 0 \le \xi \le \xi_c \\ &\frac{d^4 w_2}{d\xi^4} - M^2 \frac{d}{d\xi}\left(\left(r(1-\xi) + \frac{1}{2}(1-\xi^2)\right)\frac{dw_2}{d\xi}\right) - \mu^2 w_2 = 0 \qquad \xi_c \le \xi \le 1 \end{aligned} \tag{5}$$

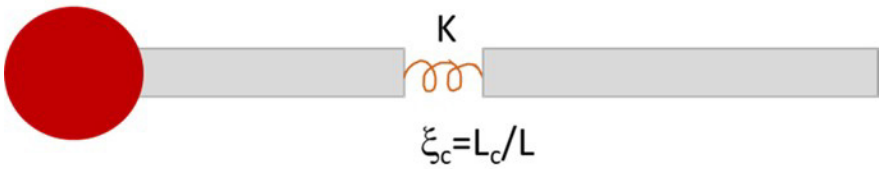

Figure 2 Schematic representation of the model of the crack in the beam

$$\frac{1}{K} = \frac{6\pi(1-\nu^2)h\phi(\alpha)}{EI}$$

$$\begin{aligned} \phi(\alpha) = {} & 0.6272\alpha^2 - 0.04533\alpha^3 + \ 4.5948\alpha^4 - 9.9736\alpha^5 + 20.2948\alpha^6 - \\ & -33.031\alpha^7 + 47.1063\alpha^8 - 40.7556\alpha^9 + 19.6\alpha^{10} \end{aligned} \tag{6}$$

where v is the Poisson's ratio of the material.

The solution of the equation requires the establishment of boundary and compatibility conditions on the cracked section, which are given by Eq. (7) and (8), respectively.

$$w_1(0) = 0;\quad \frac{dw_1(0)}{d\xi} = 0 \quad ;\ \frac{d^2 w_2(1)}{d\xi^2} = 0\ ;\ \frac{d^3 w_2(1)}{d\xi^3} = 0 \tag{7}$$

$$w_1(\xi_c) = w_2(\xi_c); \frac{dw_2(\xi_c)}{d\xi} - \frac{dw_1(\xi_c)}{d\xi} = \frac{EI}{K}\frac{d^2 w_2(\xi_c)}{d\xi^2};\ \frac{d^2 w_1(\xi_c)}{d\xi^2} = \frac{d^2 w_2(\xi_c)}{d\xi^2};\ \frac{d^3 w_1(\xi_c)}{d\xi^3} = \frac{d^3 w_2(\xi_c)}{d\xi^3} \tag{8}$$

2.2 Solution of the equation of motion of a cracked rotating Euler Bernoulli rotating beam

The equation of motion has been solved using the Frobenius series method, that allows the expression of the solution of the differential equation in the form depicted by Eq. (9).

$$f(\xi,J)=\sum_{n=0}^{\infty}a_{n+1}(J)\cdot\xi^{J+n} \tag{9}$$

The series coefficients are denoted as $a_{n+1}(J)$, where j is an indeterminate exponent. The function $f(\xi,J)$ represents both ω_1 and ω_2, since they are initially identical before applying the boundary conditions.

By substituting Eq. (9) into Eq. (5), we can derive the indicial equation and the recurrence relationship (Muñoz-Abella et al. 2022a). From these equations, the solutions $F_1(\xi)$ and $F_2(\xi)$ are calculated as a linear combination of $f(\xi,0)$, $f(\xi,1)$, $f(\xi,2)$ and $f(\xi,3)$.

$$\begin{aligned} F_1(\xi)&=C_1w_1(\xi,0)+C_2w_1(\xi,1)+C_3w_1(\xi,2)+C_4w_1(\xi,3) \qquad 0\le\xi\le\xi_c\\ F_2(\xi)&=C_5w_2(\xi,0)+C_6w_2(\xi,1)+C_7w_2(\xi,2)+C_8w_2(\xi,3) \qquad \xi_c\le\xi\le 1\end{aligned} \tag{10}$$

The constants C_1 to C_8 are calculated from the boundary and compatibility conditions Eq. (7) and (8).

To carry out the study, frequency values have been calculated, using the proposed mathematical model, for a cracked beam with the geometrical and material properties given in Table 1. On the other hand, the ranges of the variables involved in the problem are indicated in Table 2.

Table 1 Geometrical and material properties of the cracked beam.

Properties of the beam	
Length, L	0.7 m
Width, B	0.01m
Young´s modulus, E	210 GPa
Poisson´s ratio, ν	0.33
Density, ρ	7850 kg/m^3

Table 2 Range of the variables on which the frequencies of the cracked beam depend.

Range of the variables	
Slenderness, S_L	70, 120, 170 and 220
Hub radius, r	0, 0.1, 0.2 and 0.3
Rotation velocity, Ω (rad/s)	0, 2, 4, 6, 8 and 10
Crack location, ξ_c	0.1 to 0.9 each 0.1
Crack Depth, α	0, 0.1, 0.2, 0.3, 0.4 and 0.5

The direct problem has been solved as indicated obtaining the first two natural frequencies. Table 3 and Table 4 show some of the solved cases with the respective parameter values and frequencies found.

2.3 Closed-form solutions for the natural frequencies

From the 5184 computed cases (with all possible combinations of Table 2) two closed expressions have been obtained, one for each of the calculated natural frequencies μ_1 and μ_2, intended to be used in solving the inverse problem. The expressions depend on the dimensionless variables: dimensionless angular velocity (M), hub radius (r), slenderness coefficient (S_L), crack position (ξ_c) and crack depth (α) (Muñoz-Abella et al. 2022a).

First of all, six expressions for each natural frequency, which relate μ_q (q=1,2) with α, for α=0, 0.1, 0.2, 0.3, 0.4 and 0.5, respectively, are calculated. In the same order, that is $\mu_q^{\alpha_0}$, $\mu_q^{\alpha_{01}}$, $\mu_q^{\alpha_{02}}$, $\mu_q^{\alpha_{03}}$, $\mu_q^{\alpha_{04}}$ and $\mu_q^{\alpha_{05}}$. All of them have been formulated using multiple regression techniques and have similar formats, according to (11):

$$\mu_q^{\alpha}\left(M, r, S_L, \xi_c\right) = \sum_{i=0}^{i^*}\sum_{j=0}^{j^*}\sum_{k=0}^{k^*}\sum_{l=0}^{l^*} C_{ijkl}^{\alpha} \cdot M^i \cdot r^j \cdot S_L^k \cdot \xi_c^l \tag{11}$$

where I, j, k and l are the degrees of the polynomials in M, r, S_L and ξ_c, respectively. C_{ijkl} are the coefficients of the fits which are collected in a public repository (Muñoz-Abella et al. 2022b) and, finally, i*, j*, k* and l* are the values of the best fits calculated by the authors in Muñoz-Abella et al. 2022b. Finally, the general expressions of the curves relating α to μ_q, for any value of α, have the form:

$$\mu_q = \Phi_1^q \alpha^5 + \Phi_2^q \alpha^4 + \Phi_3^q \alpha^3 + \Phi_4^q \alpha^2 + \Phi_5^q \alpha^1 + \Phi_6^q \tag{12}$$

where Φ_1^q to Φ_6^q are twelve unknown coefficients, six for μ_1 and six for μ_2, that can be computed from:

$$\Phi = \Gamma^1 \mu_q$$

$$\Gamma = \begin{pmatrix} 0 & 0 & 0 & 0 & 0 & 1 \\ 0.1 & 0.1^2 & 0.1^3 & 0.1^4 & 0.1^5 & 0.1^6 \\ 0.2 & 0.2^2 & 0.2^3 & 0.2^4 & 0.2^5 & 0.2^6 \\ 0.3 & 0.3^2 & 0.3^3 & 0.3^4 & 0.3^5 & 0.3^6 \\ 0.4 & 0.4^2 & 0.4^3 & 0.4^4 & 0.4^5 & 0.4^6 \\ 0.5 & 0.5^2 & 0.5^3 & 0.5^4 & 0.5^5 & 0.5^6 \end{pmatrix} \quad \Phi = \begin{pmatrix} \Phi_1^q \\ \Phi_2^q \\ \Phi_3^q \\ \Phi_4^q \\ \Phi_5^q \\ \Phi_6^q \end{pmatrix} \quad \mu_q = \begin{pmatrix} \mu_q^{\alpha_0} \\ \mu_q^{\alpha_{01}} \\ \mu_q^{\alpha_{02}} \\ \mu_q^{\alpha_{03}} \\ \mu_q^{\alpha_{04}} \\ \mu_q^{\alpha_{05}} \end{pmatrix} \tag{13}$$

From the above equations, for any set of data (M, r, S_L, ξ_c, α), both μ_1 and μ_2 can be obtained.

3 SOLVING THE INVERSE PROBLEM

Once we have formulated the direct problem that allows us to obtain the first two natural frequencies, taking into account the characteristics of the cracked rotating beam (Tables 1 and 2), we proceed to tackle the inverse problem that consists of determining the characteristics of the crack contained in the beam (if it exists) from the knowledge of the natural frequencies of the beam by applying a novel optimisation algorithm of the type known as swarm optimisation. In this case, the algorithm based on the behaviour of rabbits, Artificial Rabbit Optimization (ARO) (Wang et al. 2022), has been chosen because it is a simple algorithm to implement and its good results have been demonstrated in very recent works such as those referred to by the developers of the algorithm (Wang et al. 2022), with some engineering examples, and by other authors such as Alamir et al. (2023) who use it for the optimization of energy management.

3.1 Artificial Rabbit Optimization (ARO)

This is a meta-heuristic algorithm used to solve optimisation problems in the field of engineering due to its simplicity, ease of implementation and efficiency. In general, the benefits of these meta-heuristic techniques lie in their randomness, which avoids local minima problems and because they are of the black box type in which the only things necessary are the input and output. These benefits make them especially interesting in nonlinear problems (Boussaïd et al., 2013 and Dhiman and Kaur 2019). Within the classification indicated by Wang et al. (2022) in their article on the development and application of the algorithm, they present it as swarm-based, in which they try to mimic the behaviour of swarms in nature. In this case, the ARO aims to mimic the survival strategies of rabbits in nature. In general terms, rabbits tend not to eat grass near their burrows, they tend to make false burrows that they do not use or use as shelter when attacked, and they adapt to choose feeding and shelter areas based on energy. The search strategy is divided into three phases: diversion for foraging, random concealment and energy reduction. The phases of the algorithm are called: exploration (detour foraging), exploitation (random hiding) and switch from exploration to exploitation (energy shrink).

The mathematic model applied is the one shown below, Wang et al. (2022), divided into the three phases indicated (Figure 3):

1. Explotarion (Detour foraging):

Each individual in the search process tends to adjust its position relative to another randomly selected individual within the swarm, incorporating a perturbation in the process.

$$x_i(t+1) = x_j(t) + R \times (x_i(t) - x_j(t)) + round(0.5 \times (0.05 + r_1)) \times n_i, \quad i,j = 1,....,n \quad j \neq i \tag{14}$$

$$R = L \times c \tag{15}$$

$$L = \left(e - e^{\left(\frac{t-1}{T}\right)^2} \right) \times \sin\left(2\pi r_2\right) \tag{16}$$

$$c(k) = \begin{cases} 1 & \text{if } k == g(l) \\ 0 & \text{else} \end{cases} \quad k = 1,...,d \text{ and } l = 1,...\left[r_3, d\right] \tag{17}$$

$$g = randperm(d) \tag{18}$$

$$n_1 \sim N\left(0,1\right) \tag{19}$$

2. Exploitation (random hiding):

To evade predators, rabbits typically excavate burrows close to their nests as a hiding strategy. The equations for this phase are:

$$B_{i,j}(t) = x_i(t) + H \cdot g \cdot x_i(t), \quad i = 1,....,n \quad and \quad j = 1,...,d \tag{20}$$

$$H = \frac{T - t + 1}{T} \cdot r_4 \tag{21}$$

$$n_2 \sim N\left(0,1\right) \tag{22}$$

$$g(k) = \begin{cases} 1 & \text{if k} == j \\ 0 & \text{else} \end{cases} \quad k = 1,...,d \tag{23}$$

In order not to be caught, the rabbits choose their hiding place randomly among the different holes. This hiding strategy can be modelled:

$$x_i(t+1) = x_i(t) + R \times (r_4 \times B_{i,r}(t) - x_i(t)), \quad i = 1,....,n \tag{24}$$

$$g(k) = \begin{cases} 1 & \text{if k} == \left[r_5 \times d\right] \\ 0 & \text{else} \end{cases} \quad k = 1,...,d \tag{25}$$

$$B_{i,r}(t) = x_i(t) + H \cdot g_r \cdot x_i(t) \tag{26}$$

When both detour foraging and random hiding are reached, the position of the ith rabbit will be:

$$x_i(t+1) = \begin{cases} x_i(t) & f(x_i(t)) \leq f(x_i(t+1)) \\ x_i(t+1) & f(x_i(t)) > f(x_i(t+1)) \end{cases} \quad (27)$$

3. Energy shrink (switch from exploration to exploitation):

A specifically designed energy factor is implemented to shift from exploration to exploitation:

$$A(t) = 4\left(1 - \frac{t}{T}\right)\ln\frac{1}{r}; \quad r \in [0,1] \quad (28)$$

3.2 Artificial Rabbit Optimization applied to crack identification in a rotating beam

The purpose of applying this optimisation algorithm is to obtain the position and depth of the crack contained in a rotating beam for which the natural frequencies of the rotating beam are assumed. The algorithm optimises by minimising the objective function (Eq. 29):

$$F_{obj} = \sqrt{\left(\mu_{1est} - \mu_1\right)^2 + \left(\mu_{2est} - \mu_2\right)^2} \quad (29)$$

where μ_{1est} (α, ξ_c) and μ_{2est} (α, ξ_c) are the first and second dimensionless frequencies calculated with the closed expressions explained in section 2.3, while μ_1 and μ_2 are the values of the dimensionless natural frequencies measured in a real system.

The closed expressions implemented in the objective function are those that provide the pair of optimal values of position, $\xi_{c\text{-}est}$, and crack depth $\alpha_{\text{-}est}$, that are sought in this identification problem.

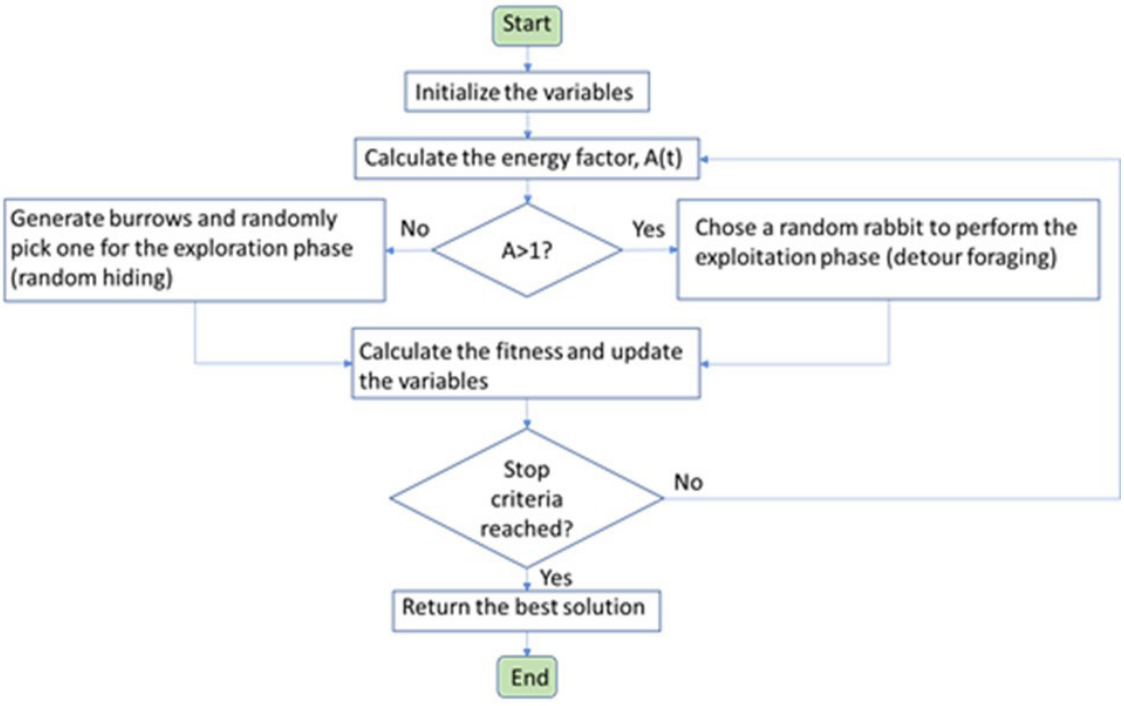

Figure 3 Flowchart of the Artificial Rabbit Optimization Algorithm.

3.3 Results of the crack identification

The frequency results obtained (Tables 3 and 4) are used to feed the algorithm that allows the estimation of the two variables that are the object of this identification problem. As mentioned before, specifically, we want to estimate the position of the crack along the length of the beam and the depth (severity) of the crack. The algorithm used is the Artificial Rabbit Optimization that has been introduced in previous sections.

The tables present several columns corresponding to 10 cases. The first column shows the rotational speed. The next two columns show the dimensionless values of the hub radius and the slenderness. The fifth and sixth columns present the dimensionless data of crack position and crack depth. Finally, the last two columns show the dimensionless natural frequencies calculated with the cracked rotating beam model (sections 2.1 and 2.2).

The cases presented in Table 3 are also used to determine the closed expressions (from section 2.3) incorporated in the optimization algorithm. Table 4 presents similar results to Table 3, but these are random data not used to obtain the mentioned closed expression.

Table 3 Selected cases and obtained frequencies.

Selected cases and frequencies							
cases	**Ω (rad/s)**	**r**	**S_L**	**ξc**	**α**	**μ_1**	**μ_2**
1	6	0.2	120	0.7	0.4	3.512	21.447
2	6	0	120	0.5	0.5	3.446	20.293
3	2	0	70	0.2	0.4	3.238	22.019
4	8	0	70	0.2	0.2	3.450	22.031
5	3	0.3	170	0.8	0.2	3.518	22.006
6	0	0.1	220	0.1	0.4	3.385	21.744
7	6	0.3	170	0.3	0.4	3.431	21.836
8	2	0.1	70	0.6	0.5	3.432	19.405
9	6	0.1	220	0.2	0.3	3.479	22.042
10	10	0.2	70	0.3	0.1	3.506	22.015

Table 4 Selected random cases and obtained frequencies.

Selected random cases and frequencies							
Cases	**Ω (rad/s)**	**r**	**SL**	**ξc**	**α**	**μ_1**	**μ_2**
R1	5.4	0.12	85	0.21	0.17	3.478	22.035
R2	9.6	0.23	210	0.58	0.34	3.541	21.661
R3	5.8	0.08	132	0.68	0.42	3.512	21.344
R4	4.6	0.27	113	0.78	0.37	3.516	21.809
R5	2.1	0.12	75	0.43	0.27	3.476	21.479
R6	3.4	0.01	216	0.89	0.16	3.519	22.035
R7	8.5	0.17	98	0.22	0.48	3.222	22.036
R8	1.5	0.25	106	0.77	0.27	3.515	21.899
R9	6.8	0.16	121	0.38	0.08	3.518	22.016
R10	7.3	0.07	89	0.14	0.41	3.237	21.747

Table 5 Selected cases, obtained frequencies and estimations.

Selected cases and estimations								
Cases	**ξc**	**α**	**ξ_c-est**	**α-est**	**Dif ξ_c**	**Dif α**	**ε%(ξ_c)**	**ε%(α)**
1	0.7	0.4	0.683	0.377	0.017	0.023	2.43	5.75
2	0.5	0.5	0.508	0.498	-0.008	0.002	-1.60	0.40
3	0.2	0.4	0.227	0.419	-0.027	-0.019	-13.50	-4.75
4	0.2	0.2	0.178	0.193	0.022	0.007	11.00	3.50
5	0.8	0.2	0.827	0.270	-0.027	-0.070	-3.37	-35.00
6	0.1	0.4	0.100	0.394	0.000	0.006	0.00	1.50
7	0.3	0.4	0.294	0.403	0.006	-0.003	2.00	-0.75
8	0.6	0.5	0.601	0.500	-0.001	0.000	-0.17	0.00
9	0.2	0.3	0.228	0.301	-0.028	-0.001	-14.00	-0.33
10	0.3	0.1	0.295	0.099	0.005	0.001	1.67	1.00

Table 6 Selected cases, obtained frequencies and estimations.

Selected random cases and estimations								
Cases	**ξc**	**α**	**ξc-est**	**α-est**	**Dif ξc**	**Dif α**	**ε%(ξc)**	**ε%(α)**
R1	0.21	0.17	0.184	0.156	0.026	0.014	12.38	8.24
R2	0.58	0.34	0.622	0.364	-0.042	-0.024	-7.24	-7.06
R3	0.68	0.42	0.720	0.469	-0.040	-0.049	-5.88	-11.67
R4	0.78	0.37	0.773	0.359	0.007	0.011	0.90	2.97
R5	0.43	0.27	0.432	0.268	-0.002	0.002	-0.47	0.74
R6	0.89	0.16	0.804	0.107	0.086	0.053	9.66	33.13
R7	0.22	0.48	0.221	0.477	-0.001	0.003	-0.45	0.63
R8	0.77	0.27	0.730	0.205	0.040	0.065	5.19	24.07
R9	0.38	0.08	0.415	0.058	-0.035	0.022	-9.21	27.50
R10	0.14	0.41	0.130	0.394	0.010	0.016	7.14	3.90

Table 5 shows the results of applying the ARO algorithm to the cases and results of Table 3. The table shows not only the results of the estimation of the variables but also the difference with the initial values and the percentage error, calculated according to (30).

$$\varepsilon\% = \frac{true\ value - estimated\ value}{true\ value} 100 \tag{30}$$

It can be seen that the differences are very small. In the most unfavourable case, this difference is 0.028 in the estimation of the position (case 10) and 0.07 in the estimation of the depth of the crack (case 5), this result being conservative. Regarding the percentage errors, the highest values occur when the crack is positioned near ξc=0.2 or in proximity to the free end of the beam. This situation is best explained by examining Figure 4, which shows how μ_1 (a) and μ_2 (b) vary as a function of ξc for a given case (equal values of angular velocity, hub radius, slenderness coefficient, crack position) and different crack depths values.

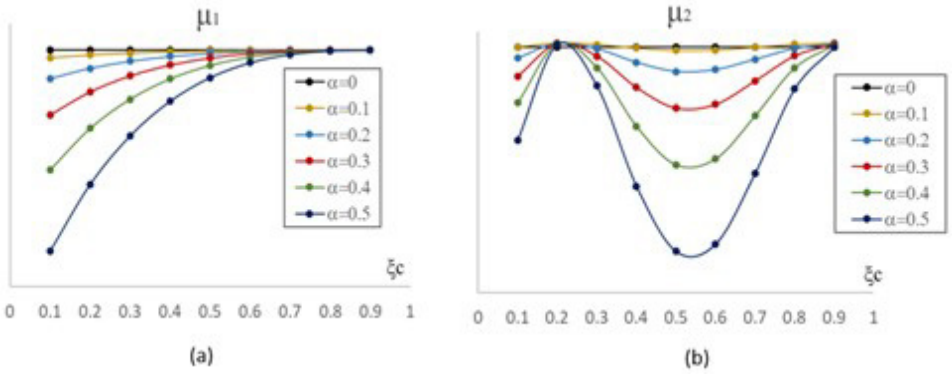

Figure 4 Dimensionless natural frequencies vs. crack position for a given case and different crack depths. (a) μ_1 (b) μ_2

As can be seen, in the vicinity of ξc=0.2 the values of μ_2 are practically the same, regardless of the α value. The same is true for μ_1 when the crack is close to the free end of the beam. However, although this circumstance complicates the implementation of the algorithm and the procedure offers less precise estimates, they are considered good enough, since, for example, in the worst case a value of alpha=0.27 is estimated instead of 0.2, which is a difference very small according to the purpose of the work. In this way, the analytical model for calculating the frequencies of a rotating cracked Euler Bernoulli beam (Muñoz-Abella et al. 2022a) is once again validated and, additionally, the opportunity of using the ARO algorithm for the identification of a crack in this type of mechanical component is verified.

To confirm the validity of the application of the optimisation method to the identification of cracks in rotating beams, the same is applied to the random data in Table 4. The results of this application are shown in Table 6. It can be seen that the estimation of both position and crack depth are somewhat less accurate than for the previous data, but

they are adjusted with admissible differences given the complexity of the problem. The largest differences are located in the case CR6 (Dif ξ_c=0.086) in the position estimation and the CR8 case (Dif α=0.065) in the depth estimation, which, as indicated above, are considered admissible values. Regarding the percentage errors, the situation is the same as explained in the case of the values in Table 5.

As an example, the diagram of the execution of the algorithm for case 1 is presented in Figure 5. As can be seen, the best fit is reached after 111 iterations. Similar results are obtained for all the other cases.

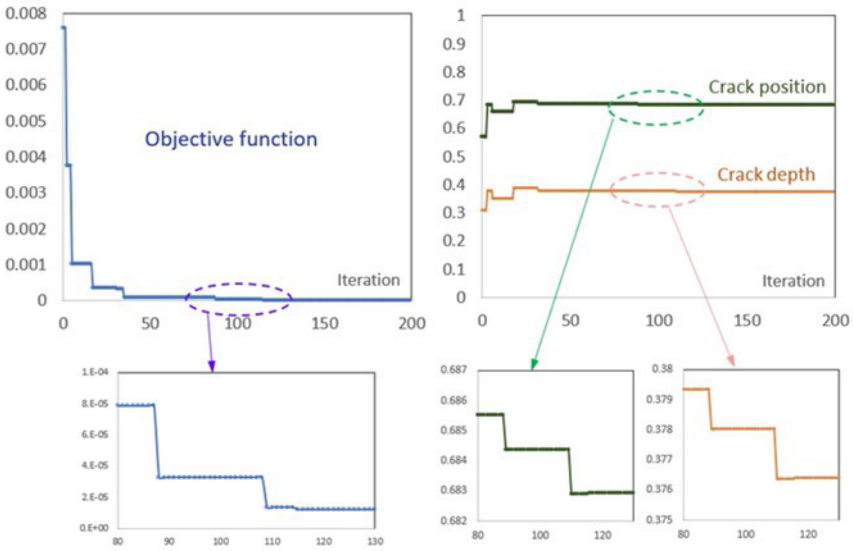

Figure 5 Crack identification ARO algorithm performance. Case 1.

4 CONCLUSION

This paper presents a summary of the initial theoretical study necessary for the subsequent practical application of an optimisation method for the identification of cracks in rotating Euler Bernoulli beams rotating at low speeds, a simplification of the operation of more complex devices such as wind turbine blades. The proposed identification methodology focuses on the use of a novel optimisation algorithm: Artificial Rabbit Optimisation (ARO) (Wang et al. 2022). This is a meta-heuristic algorithm that mimics the survival behaviour of rabbits. With the application of the algorithm, unlike other methodologies that require intermediate steps (Muñoz-Abella et al. 2022a), the two variables to be identified are accurately estimated in a single step: position along the beam and depth of the crack. The application of the model has been carried out with two types of data: data used to obtain the behavioural model of the cracked rotating beam and random data not used to obtain the behavioural model of the cracked rotating beam. In all cases, accurate results are achieved that allow validating the use of this algorithm in health monitoring problems of this type of mechanical components in operation. The methodology presented in this paper is an initial step toward using more complex problems that incorporate the Timoshenko beam model instead of the Euler-Bernoulli model (applicable to non-slender beams), beams with variable cross-sections and the nonlinear breathing mechanism occurring on the crack surfaces.

Author's Contributions: Conceptualization, B Muñoz-Abella and L Rubio; Methodology, B Muñoz-Abella; Investigation, B Muñoz-Abella; Writing - original draft, B Muñoz-Abella and L Rubio; Writing - review & editing, B Muñoz-Abella, L Rubio and P Rubio; Funding acquisition, B Muñoz-Abella, L Rubio and P Rubio; Resources, B Muñoz-Abella, L Rubio and P Rubio; Supervision, B Muñoz-Abella.

Editor: Rogério José Marczak

References

Alamir N., Kamel S., Hassan M.H., Abdelkader S.M., (2023). An effective quantum artificial rabbits optimizer for energy management in microgrid considering demand response. Soft Computing 27:15741-15768.

Alsaiari A.O., Moustafa E.B., Alhumade H., Abulkhair H., Elsheikh A., (2023). A coupled artificial neural network with artificial rabbits optimizer for predicting water productivity of different designs of solar stills. Advances in Engineering Software 175:103315.

Banerjee A., Pohit, G., (2014). Crack detection in rotating cantilever beam by continuous wavelet transform. Applied Mechanics and Materials 592-594:2021-2025. Banerjee, J.R., Su, H. and Jackson, D.R. (2006), Free vibration of rotating tapered beams using the dynamic stiffness method. Journal of Sound and Vibration. 4-5: 1034-1054.

Bhat R.B., (1986). Transverse vibrations of a rotating uniform cantilever beam with tip mass as predicted by using beam characteristic orthogonal polynomials in the Rayleigh-Ritz Method, Journal of Sound and Vibration 105(2):199-210.

Bilotta A., Morassi A., Turco E., (2023). Damage identification for steel-concrete composite beams through convolutional neural networks. Journal of Vibration and Control 0(0) online.

Boussaïd I., Lepagnot J., Siarry P., (2013). A survey on optimization metaheuristics. Information Sciences 237:82-117.

Chen, L.W., Chen, C.L., (1988). Vibration and stability of cracked thick rotating blades. Computers & Structures 28:67-74.

Dhiman G., Kaur A., (2019). STOA: a bio-inspired based optimization algorithm for industrial engineering problems. Engineering Applications of Artificial Intelligence 8:148-174

Eberhart R., Kennedy J., (1995). A new optimizer using particle swarm theory. Proceedings of the Sixth International Symposium on Micro Machine and Human Science (MHS'95). IEEE.

Ertenlice O., Kalayci C.B., (2018). A survey of swarm intelligence for portfolio optimization: Algorithms and applications. Swarm and Evolutionary Computation 39:36-52.

Fernández-Sáez J., Morassi A., Rubio L. (2017). Crack identification in elastically restrained vibrating rods. International Journal of Non-Linear Mechanics 94:257-267.

Fernández-Sáez J., Rubio L., Navarro C., (1999). Approximate calculation of the fundamental frequency for bending vibrations of cracked beams. Journal of Sound and Vibration 225(2):345-352.

Gordan M., Razak H.A., Ismail Z., Ghaedi K., (2017). Recent Developments in Damage Identification of Structures Using Data Mining. Latin American Journal of Solids and Structures 14(13):2373-2401.

Jahangiri V., Mirab H., Fathi R., Ettefagh M.M., (2016). TLP Structural Health Monitoring Based on Vibration Signal of Energy Harvesting System. Latin American Journal of Solids and Structures 13(5): 897-915.

Karaboga D., Akay B., (2009). A comparative study of Artificial Bee Colony algorithm. Applied Mathematics and Computation 214(1):108-132.

Lee, J.W, Lee, J. Y., (2017). In-plane bending vibration analysis of a rotating beam with multiple edge cracks by using the transfer matrix method. Meccanica 52:1143–1157.

Loya J.A., Rubio L., Fernández-Sáez J., (2006). Natural frequencies for bending vibrations of Timoshenko cracked beams. Journal of Sound and Vibration 290(3-5):640-653.

Maity D., Tripathy R.R., (2005). Damage assessment of structures from changes in natural frequencies using genetic algorithm. Structural Engineering and Mechanics 19(1):21-42.

Marques D., Flor F., Medeiros R., Pagani jr. C., Tita V., (2018). Structural health monitoring of sandwich structures based on dynamic analysis. Latin American Journal of Solids and Structures 15(11): SOLMEC 2017.

Mirjalili S., Lewis A., (2016). The whale optimization algorithm. Advances in Engineering Software 95:51-67.

Mohammed A.A, Neilson R.D., Deans W.F., MacConnell P., (2014). Crack detection in a rotating shaft using artificial neural networks and PSD characterization. Meccanica 49:255-266.

Muñoz-Abella B., Rubio L., Rubio P., Montero L. (2018). Elliptical Crack Identification in a Nonrotating Shaft. Shock and Vibration 2018:4623035.

Muñoz-Abella, B., Ruiz-Fuentes, A., Rubio, P., Montero, L., Rubio, L., (2020). Cracked rotor diagnosis by means of frequency spectrum and artificial neural networks. Smart Structures and Systems 25(4):459-469.

Muñoz-Abella, B., Rubio, L., Rubio, P., (2022a). Closed-Form Solution for the Natural Frequencies of Low-Speed Cracked Euler–Bernoulli Rotating Beams. Mathematics 10:4742.

Muñoz-Abella B., Rubio L., Rubio P., (2022b). GitHub Repository. Coefficients Low-Speed EB Cracked Rotating Beam.

Muñoz-Abella B., Rubio L., Rubio P., (2023). Detection and identification of cracks in slender rotating beams at low angular speeds from modal parameters and artificial neural networks (in Spanish). Revista Iberoamericana de Ingeniería Mecánica 27(2):61-73.

Naruei I., Keynia F., (2022). Wild horse optimizer: a new meta-heuristic algorithm for solving engineering optimization problems. Engineering with Computers 38(4): S3025–S3056.

Nguyen Q.H., Nguyen L.N., Bui T.T, Tran H.N., Nguyen H.T., Nguyn T.X., (2024). An improved Artificial Rabbit Optimization for structural damage identification. Latin American Journal of Solids and Structures, in press.

Ramezani M., Bahar O., (2021). Structural damage identification for elements and connections using an improved genetic algorithm. Smart Structures and Systems 28(5):643-660.

Rubio L., (2009). An efficient method for crack identification in simply supported Euler-Bernoulli beams. Journal of Vibration and Acoustics 131(5):0510011-0510016.

Rubio L., Fernández-Sáez J., Morassi A. (2018). Identification of an open crack in a beam with variable profile by two resonant frequencies. JVC/Journal of Vibration and Control 24(5):839-859.

Shekar A.S., (2004). Crack identification in a rotor system: a model-based approach. Journal of Sound and Vibration 270(4-5):887-902.

Suh M.W., Yu J.M., Lee J. H., (2000). Crack Identification Using Classical Optimization Technique. Key Engineering Materials 183-187:61-66.

Valverde-Marcos, B., Muñoz-Abella, B., Rubio, P., Rubio, L., (2022). Influence of the rotation speed on the dynamic behaviour of a cracked rotating beam. Theoretical and Applied Fracture Mechanics 117:103209.

Wang, L., Cao, Q., Zhang, Z., Mirjalili, S., & Zhao, W. (2022). Artificial rabbits optimization: a new bio-inspired meta-heuristic algorithm for solving engineering optimization problems. Engineering Applications of Artificial Intelligence 114, 105082.

Wauer J., (1991). Dynamics of cracked rotating blades. Applied Mechanics Reviews 44:273-278.

Yang X.S., (2010). Firefly algorithm, stochastic test functions and design optimization. International Journal of Bio-inspired Computation 2(2):78-84.

Yashar A., Ferguson, N., Ghandchi-Tehrani, M., (2018). Simplified modelling and analysis of a rotating Euler-Bernoulli beam with a single cracked edge. Journal of Sound and Vibration 420:346-356.

Zhao W., Zhang Z., Wang L., (2020). Manta ray foraging optimization: An effective bio-inspired optimizer for engineering applications. Engineering Applications of Artificial Intelligence 87:103300.